J Mol Model (2011) 17:2939–2951
DOI 10.1007/s00894-011-0968-9

ORIGINAL PAPER

Analysis of *Bacillus anthracis* nucleoside hydrolase via in silico docking with inhibitors and molecular dynamics simulation

Ana P. Guimarães · Aline A. Oliveira · Elaine F. F. da Cunha · Teodorico C. Ramalho · Tanos C. C. França

Received: 10 September 2010 / Accepted: 11 January 2011 / Published online: 12 February 2011

Abstract As the enzyme nucleoside hydrolase (NH) is widely found in nature but has not yet been detected in mammals, it is considered an ideal target in the development of chemotherapy against parasitic diseases and bacterial infections like anthrax. Considering the risk that this biological warfare agent represents nowadays, the search for new drugs and new molecular targets in the development of chemotherapy against anthrax is imperative. On this basis, we performed docking studies of six known NH inhibitors at the active site of NH from *Bacillus anthracis* (*Ba*NH). Subsequently, molecular dynamics (MD) simulations of these compounds inside *Ba*NH were carried out in order to complement the docking studies and select the most promising compounds as leads for the design of potential *Ba*NH inhibitors. Most of the docking and MD results obtained agreed well with each other and showed good correlation with experimental data.

Keywords Anthrax · *Bacillus anthracis* · Nucleoside hydrolase · Docking · Molecular dynamics

A. P. Guimarães · A. A. Oliveira · T. C. C. França (✉)
Laboratory of Molecular Modeling Applied to Chemical and Biological Defense (LMCBD),
Military Institute of Engineering,
Rio de Janeiro, RJ, Brazil
e-mail: tanos@ime.eb.br

A. P. Guimarães · E. F. F. Cunha · T. C. Ramalho (✉)
Chemistry Department,
Federal University of Lavras,
Lavras, MG, Brazil
e-mail: teo@dqi.ufla.br

Introduction

Biological warfare agents consist of live microorganisms or their toxins that are used as weapons. In this context, *Bacillus anthracis*, one of the most dangerous biological agents, has been employed as a weapon by both military and terrorist groups and is capable of causing a high mortality despite the antimicrobial treatment and therapy available today [1].

B. anthracis is a Gram-positive rod-shaped bacterium found in many parts of the world that is capable of producing almost indestructible spores. These spores are resistant to disinfectants, heat, dehydration and freezing [2–4]. Infection with *B. anthracis* can occur by skin contact, inhalation or contact with the gastrointestinal tract. This bacteria can be produced in wet or dry forms and then stabilized for weaponization and dispersion by aerosol [5]. Despite the fact that anthrax therapy is now available, the risk of resistance is always present. Furthermore, it is well known that the drugs that are currently used will be ineffective against genetically modified strains of *B. anthracis* in the future. Moreover, in view of the current global geopolitical situation, with *B. anthracis* being used as a biological warfare agent for terrorist purposes, the search for new drugs and new molecular targets for anthrax therapy is imperative.

The nucleoside hydrolases (NH) of protozoa have already been extensively studied as potential targets for chemotherapeutic intervention due to the differences in the metabolism of purines between parasite and host [6–12]. These enzymes have been characterized in bacteria [13, 14], yeast [15], protozoa [10, 16], and insects [17]. The genes responsible for their expression are present in plants, amphibians and fish, but—surprisingly—no NH activity or genes that encode it have been detected in mammals to date

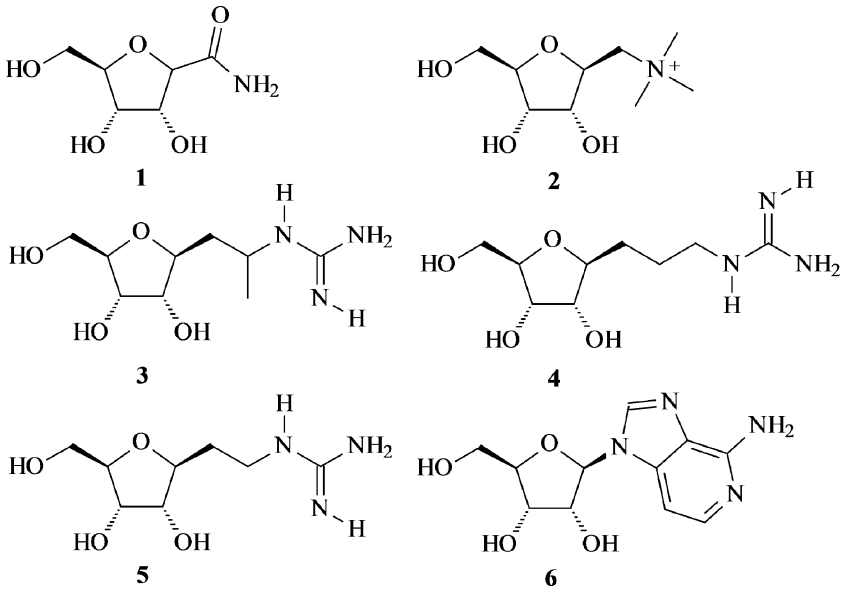

Fig. 1 Structures of the NH inhibitors studied

[12]. This means that NH is an attractive target for the development of new antimicrobial agents.

All of the NHs studied to date have been homodimers or homotetramers, and show considerable similarity in the amino acid sequences of their active sites, which indicates that they are closely related in terms of both structure and catalytic mechanism. Therefore, NH inhibitors for one species are likely to be active against many other species too [18].

In this work, we applied docking and molecular dynamics (MD) techniques in the same way as in former publications [18–26] in order to study the interactions of six *Tripanossoma vivax* NH (*Tv*NH) inhibitors developed by Goeminne et al. at the active site of *Ba*NH. The compounds were first docked inside *Ba*NH and *Tv*NH to analyze their three-dimensional arrangements as well as the main interactions with the amino acids of the active site, in order to evaluate the factors relevant to the biological activity. Subsequently, we employed MD simulations in order to evaluate the dynamic behaviors of those inhibitors and their potential as lead compounds for the design of new *Ba*NH inhibitors. The docking and MD results obtained agreed well with each other and showed a good correlation with experimental data.

Methodology

NH inhibitors studied

The compounds used in this study (Fig. 1) were selected from a number of inhibitors developed by Goeminne et al. [27, 28], whose inhibition constants (K_i) were determined

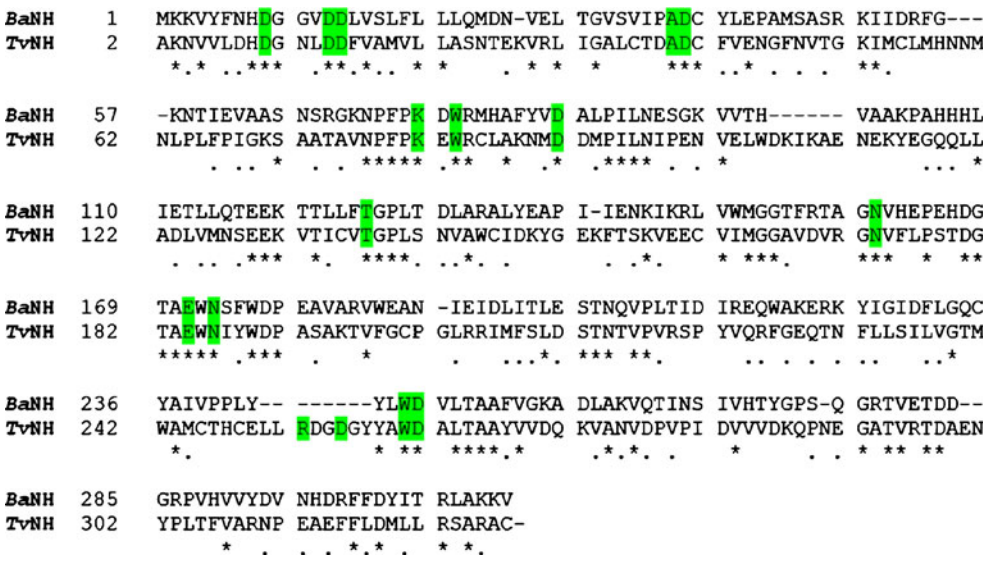

Fig. 2 Alignment of the *Ba*NH and *Tv*NH sequences. Residues belonging to the active sites are marked in *green*

Fig. 3 Superposition of the three-dimensional structures of *Ba*NH (*green*) and *Tv*NH (*purple*)

for *Tv*NH expressed in *E.coli*. In addition, we also studied, as references, the natural substrates of NH (inosine, uridine and adenosine), whose respective values of affinity with *Tv*NH (K_M) were determined by Versées et al. [29, 30].

To verify the similarity between the residues of the active sites of *Ba*NH and *Tv*NH and to determine the degree

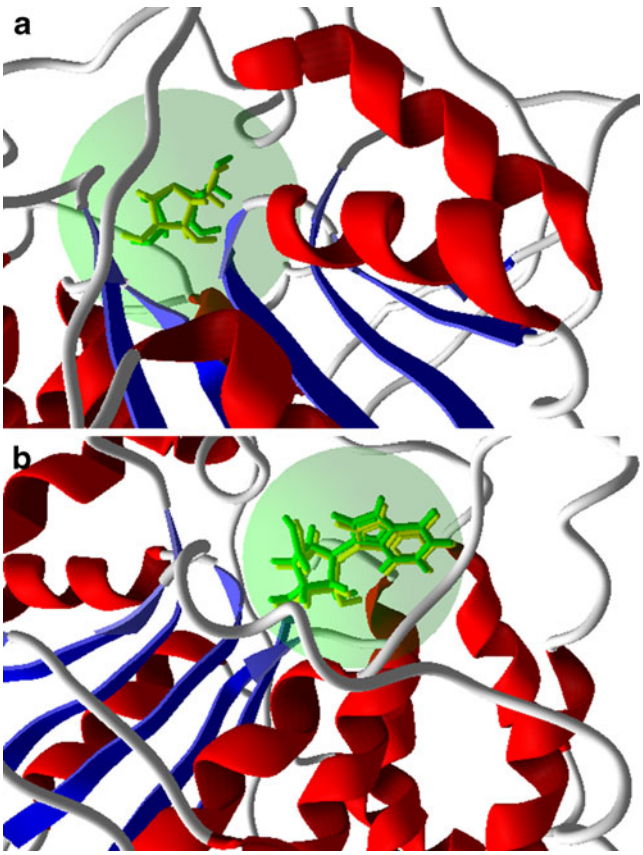

Fig. 4 Docking spheres used in the validation of the docking protocol

Table 1 Residues belonging to the active sites of *Ba*NH and *Tv*NH

*Ba*NH	*Tv*NH	*Ba*NH	*Tv*NH
Asp9	Asp10	Thr125	Thr137
Asp13	Asp14	Asn160	Asn173
Asp14	Asp15	Glu171	Glu184
Ala37	Ala39	Asn173	Asn186
Asp38	Asp40	Trp246	Trp260
Lys75	Lys81	–	Arg252
Trp77	Trp83	–	Asp255
Asp85	Asp91	Asp247	Asp261

of identity (ID) between these enzymes, we downloaded their three-dimensional structures from the Protein Data Bank (PDB) server [31] under the codes 2C40 and 2FF2, respectively, and aligned and superposed them using the SPDBViewer program [32] (see Figs. 2 and 3).

Docking energy calculations

The coordinates of the dimeric crystallographic structures of *Ba*NH and *Tv*NH downloaded from the PDB [31] are both complexed with the cofactor Ca^{+2} and, regarding the ligand, *Ba*NH is complexed with ribose while *Tv*NH is complexed with immucillin H. The function of the cofactor Ca^{+2} is to anchor the ribose portion of the substrates inside the NH active site [27–30]. For this reason, most of the NH inhibitors also have a ribose portion or a suitable isosteric group to perform this function. All of the inhibitors studied here present a ribose portion (see Fig. 1), so they are not expected to show any differences in their interactions with the cofactor.

Considering that the monomers are identical and independent of each other, we selected only monomer A from each enzyme to perform our docking and MD studies. This procedure reduced the computation time by half. Also, the co-crystallized water molecules were removed from both monomers using the software Molegro Virtual Docker (MVD®) [33].

The three-dimensional structures of each compound in Fig. 1 were built using the program PC Spartan Pro® [34], and their partial atomic charges were calculated by the PM3 semi-empirical method. The compounds were docked in the *Ba*NH and *Tv*NH binding sites using MVD® [33] inside a restriction sphere of radius 7 Å and considering the residues within a radius of 11 Å to be flexible. Due to the stochastic nature of the docking algorithm, about 20 runs were performed for each compound and 30 poses (conformation and orientation of the ligand) were returned to the analysis of the overlap and the ligand–protein interactions with the ribose and immucillin H structures present in the crystal structures of *Ba*NH and *Tv*NH, respectively. The best pose

Table 2 Docking results for the compounds docked in *Ba*NH and their *Ki* values with *Tv*NH

Compound	Residue	Dist. (Å)	Energy (kcal mol^{-1})	Intermolecular energy (kcal mol^{-1})	H-bond energy (kcal mol^{-1})	[a]K_i (μM)
1	Asp247	3.42	−0.10			
		3.19	−2.03			
	Asn160	3.43	−0.86			
	Glu171	2.68	−2.50	−71.18	−13.00	4.50×10^3
	Asn173	2.78	−2.50			
	Thr125	3.07	−2.50			
	Asp38	3.09	−2.50			
2	Glu171	2.76	−2.50			
	Asn173	2.92	−2.50			
	Thr125	3.29	−1.52			
	Asp247	3.28	−0.10	−76.77	−13.91	2.28×10^3
		3.12	−2.11			
		2.96	−2.50			
	Asp14	3.23	−1.83			
	Asp9	2.40	−0.85			
3	Asn160	3.54	−0.28			
		3.23	−1.87			
	Glu171	2.41	−0.90			
	Asn173	2.98	−0.94			
		3.01	−0.84	−85.89	−10.79	6.85×10^2
	Asp247	2.65	−2.50			
	Asp14	3.42	−0.87			
	Asp13	3.31	−1.44			
	Trp77	3.57	−0.01			
4	Asn160	3.34	−1.28			
	Asn173	2.82	−1.65			
	Asp247	2.95	−2.50			
	Asp14	3.50	−0.49	−91.57	−10.78	6.77×10^2
	Asp38	3.08	−2.50			
	Trp–77	3.13	−2.37			
5	Asn173	3.08	−0.68			
		3.31	−1.46			
		3.06	−2.50			
	Thr125	3.45	−0.75	−93.77	−13.03	3.09×10^2
	Asp247	3.18	−1.68			
		3.21	−0.97			
	Asp13	2.78	−2.50			
		3.09	−2.50			
6	Asn160	3.37	−1.15			
		3.38	−0.11			
	Glu171	3.11	−2.46			
	Asn173	2.97	−2.50			
	Thr125	3.25	−1.73			
	Asp247	3.35	−2.50			
	Asp38	2.95	−2.50	−114.42	−15.18	2.00×10^{-1}
	Val12	2.95	−2.50			
	His80	2.75	−2.50			
	Trp77	3.55	−0.33			

[a] Experimental data [19, 20]

of each compound was selected for the subsequent MD simulation steps.

To validate the docking protocol, we first performed the docking simulation at the active sites of *Ba*NH and

Table 3 Docking results and K_i values for the compounds studied docked in *Tv*NH

Compound	Residue	Dist. (Å)	Energy (kcal mol^{-1})	Intermolecular energy (kcal mol^{-1})	H-bond energy (kcal mol^{-1})	[a]K_i (μM)
1	Asp261	3.09	−2.18			
		3.14	−1.44			
	Glu184	3.17	−2.12			
	Asn186	2.78	−2.50			
		3.50	−0.30	−72.43	−16.36	4.50×10^3
		2.48	−0.24			
	Thr137	2.66	−2.50			
	Asp40	3.19	−2.03			
		2.60	−2.49			
	Asn12	3.44	−0.55			
2	Glu184	3.11	−2.44			
	Asn186	3.05	−2.50			
	Asp14	2.91	−2.50			
	Asp10	3.15	−2.26			
	Asp261	3.12	−2.42	−86.61	−18.50	2.28×10^3
		2.97	−2.50			
	Asp15	3.28	−1.59			
	Asp40	2.97	−0.95			
		3.33	−1.35			
3	Asn173	3.26	−0.75			
	Tyr257	3.28	−0.28			
	Asn186	2.43	−0.24			
	Asn12	2.35	−0.40			
	Asp261	2.90	−2.50	−84.99	−11.79	6.85×10^2
	Asp15	3.53	−0.35			
	Asp14	3.12	−2.35			
	Asp40	3.09	−2.50			
		3.02	−2.41			
4	Asn173	3.49	−0.56			
		3.49	−0.51			
	Thr137	3.41	−0.93			
	Glu184	2.90	−2.50	−86.09	−9.74	6.77×10^2
	Asn186	2.41	−0.13			
	Asp261	3.05	−2.50			
	Asp15	3.49	−0.53			
	Asp14	3.47	−0.33			
		3.33	−1.30			
	Trp185	2.88	−0.45			
5	Asn186	2.77	−0.98			
	Thr137	3.48	−0.59			
	Asp261	3.11	−2.43			
	Asp14	3.11	−2.23	−89.04	−15.84	3.09×10^2
	Asn12	2.93	−2.50			
	Asp40	3.13	−2.36			
		3.21	−0.10			
		3.30	−1.49			
	Asp15	3.21	−1.90			
	Asn173	3.26	−1.06			
6	Arg252	2.83	−2.50			
		3.50	−0.28			
	Tyr257	2.77	−2.50			
	Asn186	1.99	−2.64			
		2.87	−1.67			
	Thr137	2.39	−0.78			
	Asp261	3.11	−2.47	−111.97	−15.28	2.00×10^{-1}

Table 3 (continued)

Compound	Residue	Dist. (Å)	Energy (kcal mol^{-1})	Intermolecular energy (kcal mol^{-1})	H-bond energy (kcal mol^{-1})	[a]K_i (μM)
		3.26	−0.72			
		3.10	−2.50			
	Asp40	3.44	−0.81			
	Asp14	3.01	−2.50			
	Asp15	3.36	−1.21			

[a] Experimental data [19, 20]

*Tv*NH and compared the results to the crystallographic structures (re-docking). The coordinates for *Ba*NH were: x=16.43, y=−28.41 and z=−18.44 with a docking sphere radius of 7 Å, while for *Tv*NH, the coordinates were: x=−26.81, y=−10.26 and z=−21.06, with a docking sphere radius of 6 Å.

MD simulations

Before performing the MD simulations, it was necessary to parameterize the ligands so that they could be recognized by the force field GROMOS96 from the program GROMACS 4.0 [35]. The parameterization was carried out in the Dundee PRODRG server [36], and the charge distributions were calculated by the chelpG method at HF/6-31G(d,p) using the Gaussian 98® [37] program. The enzyme/Ca^{+2}/ligand com-

Table 4 Docking results and K_M values for the substrates studied

Compound	Residue	Dist. (Å)	Energy (kcal mol^{-1})	Intermolecular energy (kcal mol^{-1})	H-bond energy (kcal mol^{-1})	[a]K_M (μM)
Inosine	Asn160	3.16	−2.21			
	Glu171	3.80	−2.50			
	Asn173	2.79	−2.50			
	Thr125	3.23	−1.83			
	Asp38	3.22	−1.91	−110.57	−13.33	5.37
	Asp247	3.50	−0.09			
		3.29	−1.53			
	His80	2.77	−0.77			
Uridine	Asn160	3.43	−0.86			
	Asn173	3.14	−2.32			
		3.27	−0.29			
	Asp38	2.73	−2.50	−91.32	−9.15	586
	Tyr243	3.10	−2.50			
	His80	3.30	−0.68			
Adenosine	Asn173	2.78	−2.50			
	Thr125	3.23	−1.86			
	Asp247	3.58	−0.01	−106.97	−10.13	8
		3.34	−1.31			
	Asp38	2.91	−2.50			
	His80	3.21	−1.95			

[a] Experimental data [21]

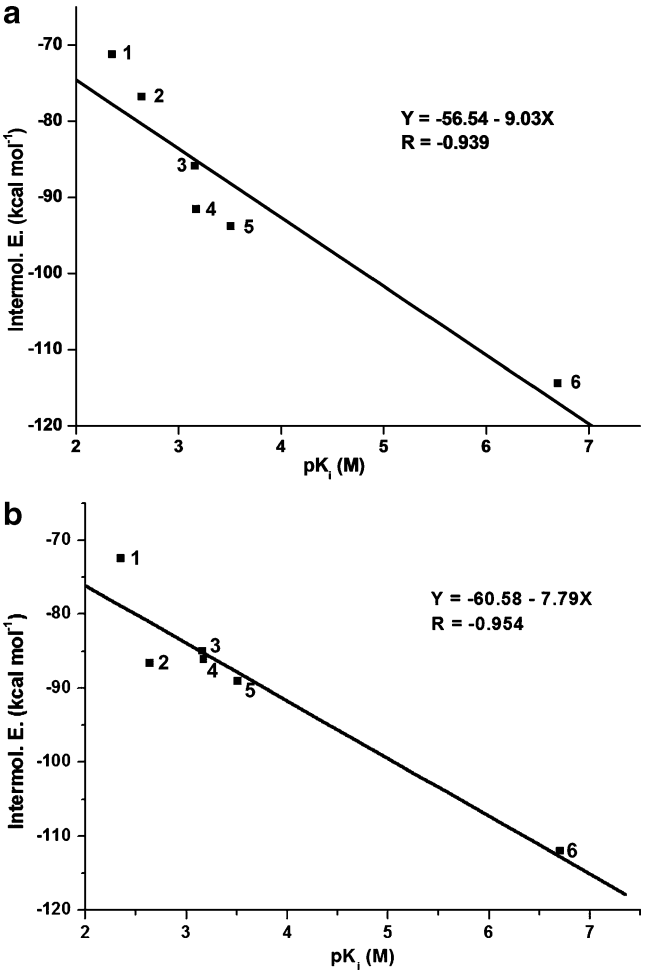

Fig. 5a–b Correlation between the intermolecular energies, calculated by MVD, and the K_i values of each compound studied, for *Ba*NH (**a**) and *Tv*NH (**b**)

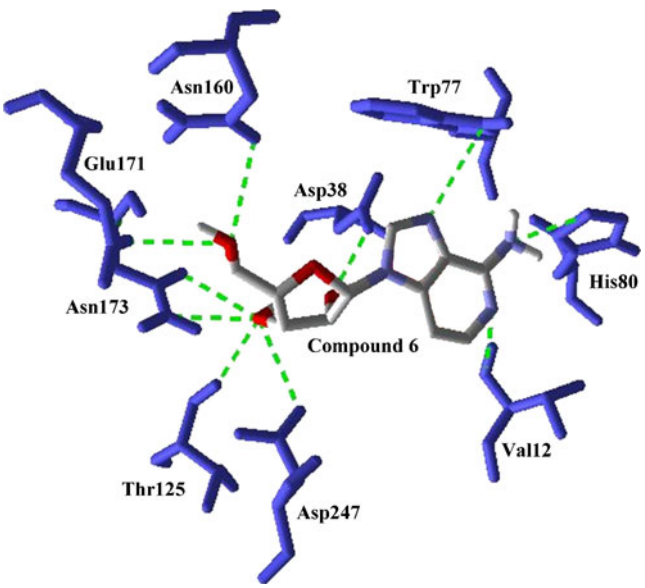

Fig. 6 Interactions between compound **6** and the residues of the active site of *Ba*NH

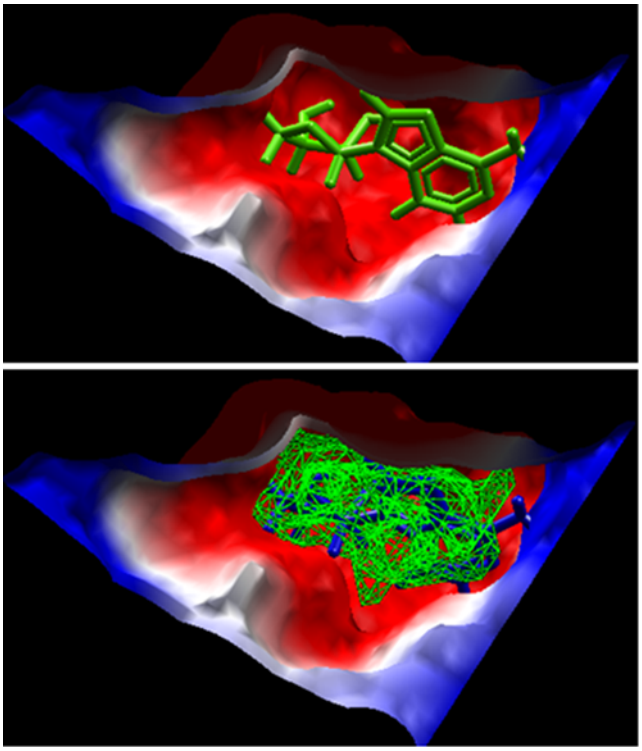

Fig. 7 Best conformation of compound **6** inside the active site of *Ba*NH. *Red* hydrophilic regions, *blue* hydrophobic regions, *green* the cavity

plexes were simulated using the GROMACS 4.0 package [35], in cubic boxes approximately 365,000 nm^3 in volume that contained around 10,600 water molecules. These systems were minimized using the force field GROMOS 96 [35]. The minimization algorithms used were steepest descent with ligand position restrained (PR) and a convergence criterion of 100.00 kcal mol^{-1} $Å^{-1}$, followed by steepest descent without PR, conjugate gradients and, finally, quasi-Newton–Raphson until an energy of 1.00 kcal mol^{-1} $Å^{-1}$. The minimized complexes were then subjected to MD simulations in two steps. Initially, we performed 500 ps of MD at 300 K with PR for the entire system, except for the water molecules, in order to ensure that the solvent molecules are balanced around the residues of the protein.

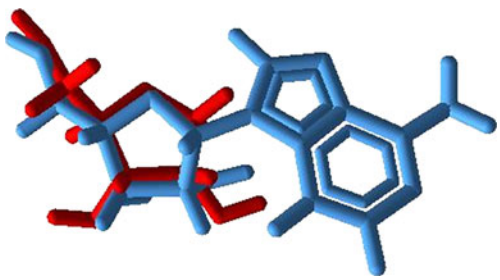

Fig. 8 Superposition of the best conformation of compound **6** (*blue*) and ribose (*red*) after docking

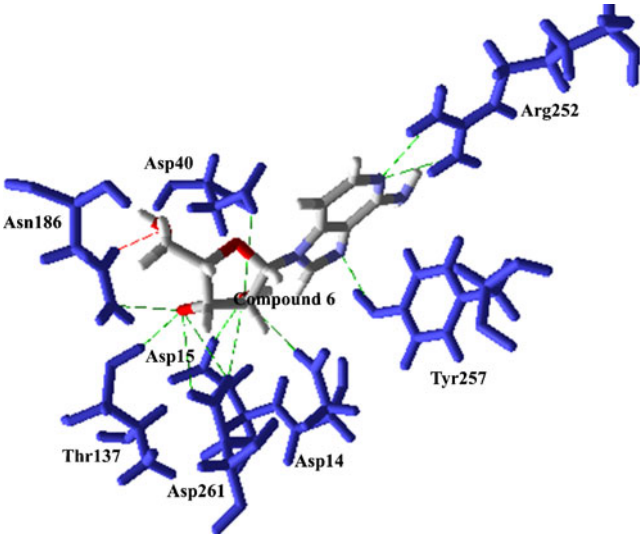

Fig. 9 Interactions between compound **6** and the residues of the active site of *Tv*NH

Subsequently, 6.0 ns of MD was performed at 300 K without any restriction, using 2 fs of integration time and a cutoff of 10 Å for long-distance interactions. A total of 300 conformations were obtained during each simulation. In this step, the lists of pairs (pairlists) were updated every 500 steps, all Arg and Lys residues were assigned with positive charges, and the residues Glu and Asp were assigned with negative charges.

To analyze the structures generated after the optimization and MD steps, we used the VMD [38] and SPDBViewer [31] software packages. Plots of the variations in the total energy, distances, RMSD and H-bonds formed as the MD simulation proceeded were generated with the Origin® software [39]. Qualitative spatial RMSD pictures were generated in MolMol [40], and the frames of the MD simulations were generated in PyMOL [41].

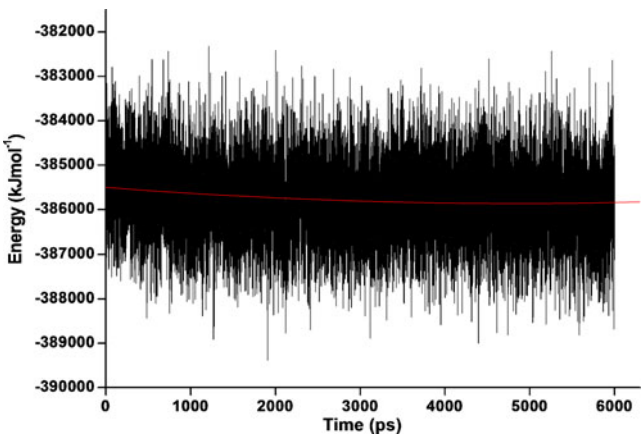

Fig. 10 Variation in total energy for the system *Ba*NH/compound **6** during the MD simulation

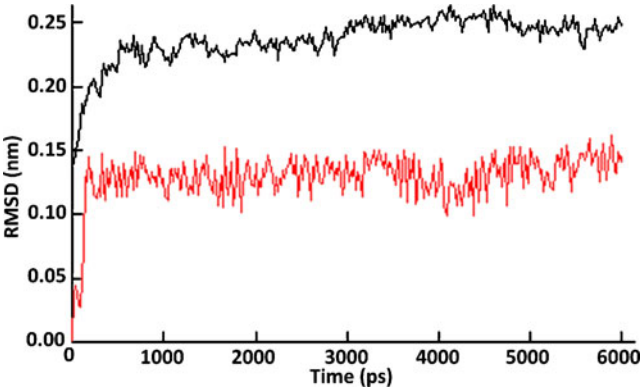

Fig. 11 Temporal RMSD values for the system *Ba*NH/compound **6**. *Black line Ba*NH, *red line* compound **6**

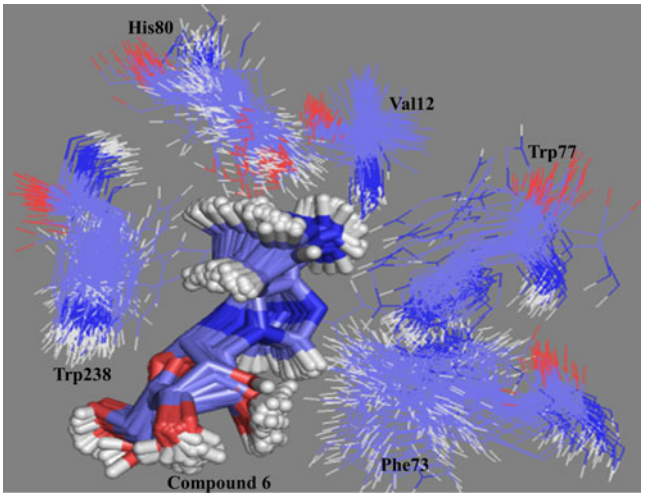

Fig. 13 Frames of compound **6** in the active site of *Ba*NH during the 6.0 ns of MD simulation

Results and discussion

Docking studies

Figure 4 shows the re-docking results for the best-docked structures of ribose and immucillin H inside *Ba*NH and *Tv*NH. The RMSDs for the superpositions of the non-hydrogen atoms were 1.000 Å for *Ba*NH and 0.579 Å for *Tv*NH, respectively. Bearing in mind that an RMSD value of less than 2.000 Å is considered acceptable [42–44], these results validate the docking protocol used.

Analysis of the ID between the *Ba*NH and *Tv*NH active sites points to high similarity. Among a total of 16 residues, 14 are identical. As can be seen in Table 1 and from the alignment in Fig. 2, the only residues of the *Tv*NH active site that were not observed in *Ba*NH are Arg252 and Asp255. These residues belong to a loop at the entrance of the active site that was not observed in *Ba*NH (see Fig. 3)

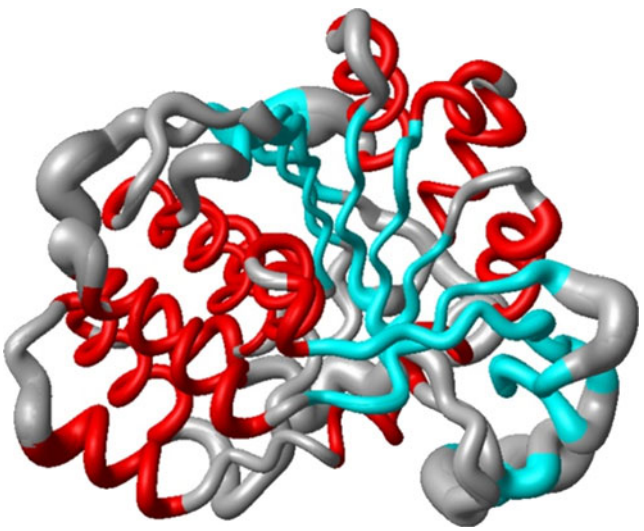

Fig. 12 Qualitative illustration of the spatial RMSD for the system *Ba*NH/compound **6**. Compound **6** was omitted for a better visualization

and, according to Versées et al. [30], they are related to the mechanism of action of NHs through secondary interactions mediated by water molecules. As will be fully discussed later, the results of the docking and MD studies revealed that Asp255 was not able to interact with any of the compounds studied, while Arg252 interacted only with compound **6**. However, the absence of these interactions in *Ba*NH, however, was compensated for by Val12 and His80. Thus, taking into account these results, and the great similarity between the active sites, we propose that these *Tv*NH inhibitors could be used as leads in the drug design of *Ba*NH inhibitors.

The ligand–protein interaction energies (electrostatic and H-bond) were calculated in order to get a better understanding of the variations between the binding modes of each compound and the molecular factors responsible for the activity. Tables 2 and 3 list the residues present in these interactions, their distances to the ligands, the energies, and the experimental inhibition constants obtained for *Tv*NH by Goeminne et al. [27, 28], while Table 4 lists the reference docking results for the natural substrates inside *Ba*NH. From Table 2 and Fig. 5a, it is clear that there is a very good correlation between the theoretical results obtained and the experimental data. Analyzing the plot in Fig. 5b, we can also see that the same correlation observed for *Tv*NH also exists for *Ba*NH. These results strengthen our hypothesis that *Tv*NH inhibitors could also work as *Ba*NH inhibitors.

The inhibitor with the smallest K_i value (compound **6** in Tables 2 and 3)—which was considered to be the most promising for *Tv*NH from an experimental perspective—yields the lowest interaction energies with both *Tv*NH and *Ba*NH, showing high stability at both active sites. It interacts with *Ba*NH through nine H-bonds, the same number observed for inosine (Tables 3 and 4). However,

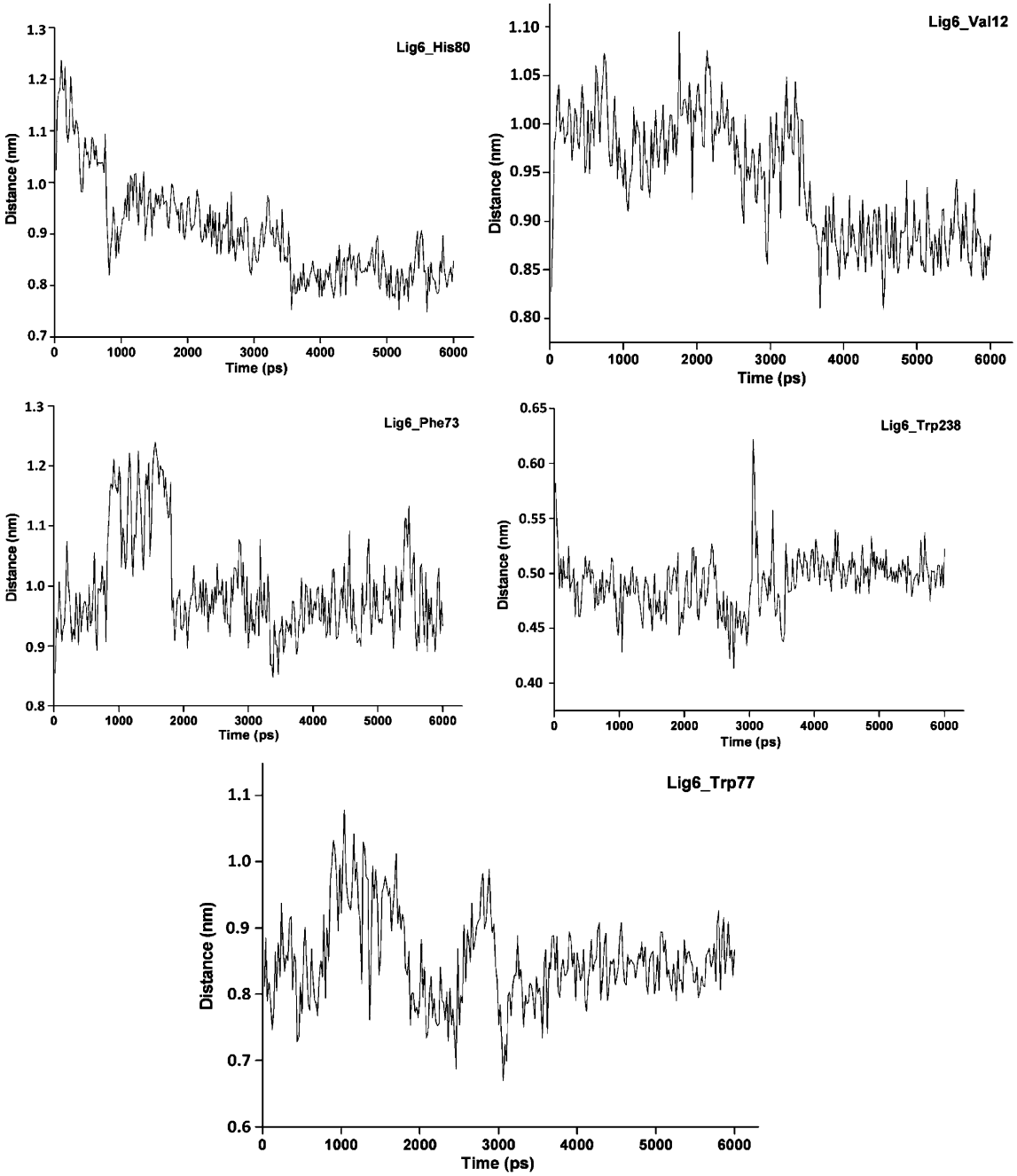

Fig. 14 Variations in the distances from compound **6** to the residues His80, Val12, Phe73, Trp238 and Trp77 during the 6.0 ns of MD simulation

the distances and energy values are different, and the interactions with the residues Asp38, His80 and Asp247 are the most stable. In addition, H-bonds were observed with Val12 and Trp77, justifying the best docking results for compound **6** (intermolecular energy of −114.42 kcal mol^{-1} and total H-bond energy of −15.18 kcal mol^{-1}) relative to inosine (intermolecular energy of −110.57 kcal mol^{-1} and total H-bond energy of −13.33 kcal mol^{-1}). Compound **6** was more effective than adenosine, showing stronger interactions (Tables 3 and 4). Moreover, compound **6** interacts with four additional residues (Val12, Trp77, Asn160, and Glu171) when compared to adenosine. The interactions of compound **6** with residues of the *Ba*NH active site are illustrated in Fig. 6. As can be seen, besides undergoing various stable interactions with the amino acids of the active site, this compound also shows good orientations at the binding sites, occupying the whole cavity (Fig. 7) and adopting a conformation similar to ribose (Fig. 8).

Regarding the docking results of compound **6** inside *Tv*NH, we observed the existence of twelve H-bonds, with most of the residues observed for *Ba*NH (Tables 2 and 3).

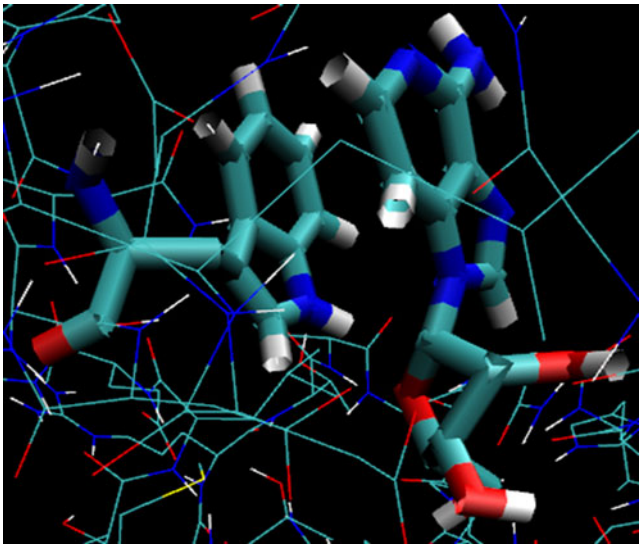

Fig. 15 Hydrophobic interactions between compound **6** and Trp238

However, the distances and energy values were different, and the interactions with the Asp14, Arg252, Tyr257 and Asp261 residues were the most stable. The strong interactions observed with Arg252 and Tyr257 justify the better docking results for compound **6** (intermolecular energy of −111.97 kcal mol^{-1} and total H-bond energy of −15.28 kcal mol^{-1}) relative to the others. As mentioned before, it was observed that compound **6** was the only one that was able to interact with Arg252. This happens through H-bonding between the N atom of the piridinic ring and the N atoms of the side chain of Arg252 (Fig. 9). This interaction, which is very important to the stabilization of the nucleobase portion inside the active site, is not observed in *Ba*NH once this enzyme does not have a residue equivalent to Arg252. On the other hand, it was observed that compound **6** finds a way to compensate for this quite well by undergoing

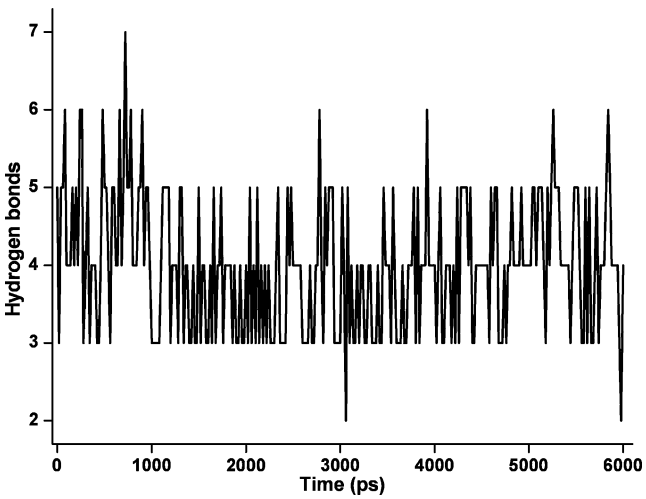

Fig. 16 Number of H-bonds observed between compound **6** and *Ba*NH during the 6.0 ns of MD simulation

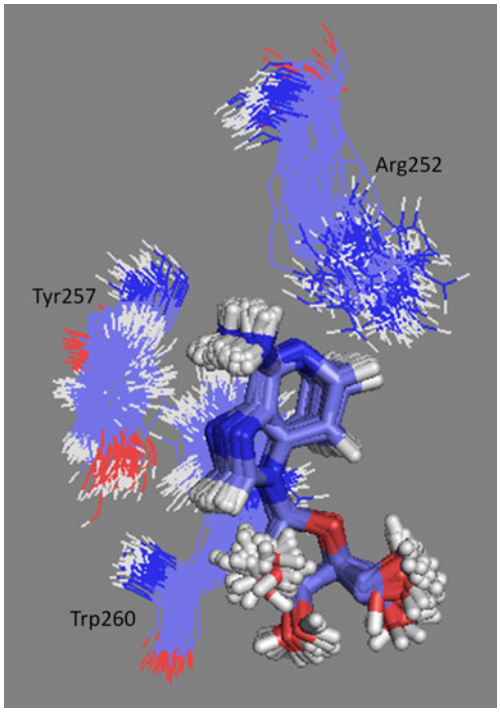

Fig. 17 Frames of compound **6** in the active site of *Tv*NH during the 6.0 ns of MD simulation

equivalent interactions with Val12 and His80 and slightly changing the position of the piridinic ring (see Fig. 6).

The compound with the highest K_i value (compound **1** in Tables 2 and 3) showed the highest intermolecular energy in both enzymes, suggesting that this ligand does not interact as strongly with the enzymes as it is less stable inside the active site, suggesting that it is a less efficient *Ba*NH inhibitor. Compound **1** interacts with *Ba*NH through seven H-bonds with the same residues observed for *Tv*NH, except for the weak interaction formed with Asn12 (Tables 2 and 3). Aside from this, the docking results (data not shown) also indicated that this compound does not adopt an appropriate position within the cavity, because the amide group shows no H-bond interactions with the residues of the active sites. Among the inhibitors proposed by Goeminne et al. [27, 28], compound **1** presented the worst intermolecular and total H-bond energy values (−71.18 kcal mol^{-1} and −13.00 kcal mol^{-1}, respectively).

Molecular dynamics simulations

After the docking studies, compounds **1**–**6** and the natural substrates were submitted to 6.0 ns of MD simulations. The goal of these simulations was to observe the dynamic behavior of these compounds in the active sites of *Ba*NH and *Tv*NH, in order to compare this behavior to the docking results and get additional information supporting the proposal of new potential inhibitors for *Ba*NH.

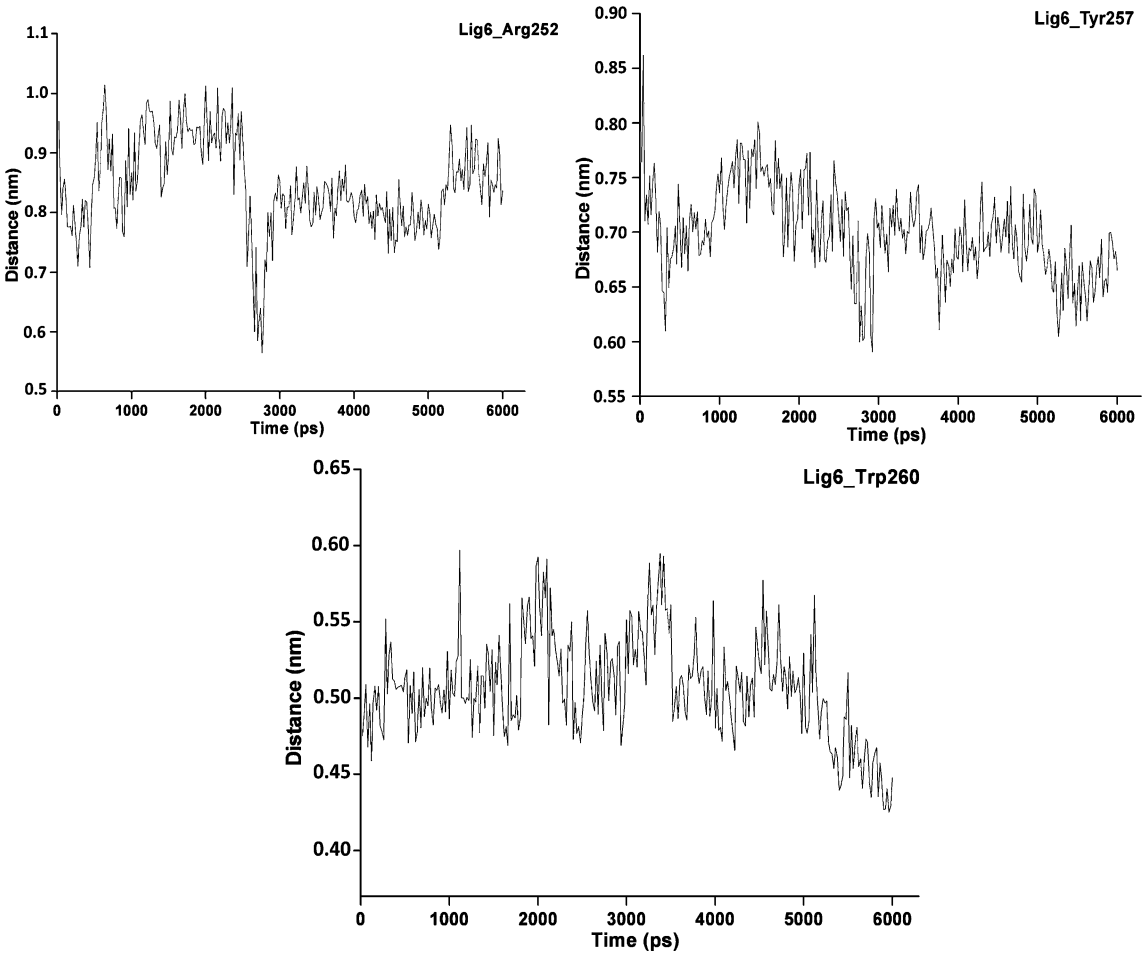

Fig. 18 Variations in the distances from compound **6** to the residues Arg252, Asp255 and Trp261 during the 6.0 ns of MD simulation

The graphs for the variation in the total energy with the dynamics showed that the total energy tends to stabilize after 2.0 ns of simulation (as shown for the system *Ba*NH/compound **6** in Fig. 10); the energy variation is about −0.04 kJ mol^{-1}, indicating that the average energy remains constant, thus suggesting structural stabilization. The same behavior was observed for all 18 systems simulated.

RMSD analysis can give an idea of how much the three-dimensional structure fluctuates over time, and it allows local fluctuations to be monitored; for example, the residues with the highest mobility during the MD simulation. The temporal RMSD calculations were performed on all of the atoms of each complex to give 300 frames every 20 ps during the 6.0 ns of simulation. Considering that the complexes could fluctuate in the box, each frame was adjusted by the least squares method to the previous one to calculate the standard deviation. In Fig. 11, we can observe the equilibration for the simulation of the system *Ba*NH/compound **6** during the initial 200 ps. This behavior was common to all simulations, with deviations never exceeding 0.33 nm (3.5 Å) and 0.31 nm (3.1 Å) for the protein and ligand, respectively. This result suggests that the compounds fit well inside the active site during the 6.0 ns of simulation, showing system stabilization and confirming the results obtained from the total energy calculations described previously. The spatial RMSD of each amino acid was also calculated, as illustrated in Fig. 12. This provides a qualitative and quantitative view of all regions of the protein during the dynamics. We can see that the regions that moved the most during the MD simulations (i.e., had the largest RMSD values and show the greatest tube thickening in the figure) correspond to the C- and N-terminal extremities and the loop regions. Moreover, the residues in the active site region, the alpha helices, and the beta sheets presented the lowest fluctuations, indicating that these were the most stable regions, as expected. The behavior observed in the temporal and spatial RMSD calculations was common to all 18 systems simulated.

To facilitate the visualization of the dynamic behavior of each inhibitor within the active site, we selected and evaluated the variations in the distances of the residues that were directly involved in interactions with each inhibitor in each system, based on the results obtained in

the docking studies. In general, the main interactions observed in the docking studies were also seen in the MD simulations, and there were no significant differences between *Ba*NH and *Tv*NH for all nine ligands aside from compound **6**. Because of this, as well as the fact that compound **6** was the one that presented the most interactions with the active sites, we will only discuss this compound in more detail here.

The sequence of frames from the MD simulation of compound **6** inside *Ba*NH, presented in Fig. 13, shows that this compound remains stabilized inside the active site, where it interacts with residues Val12, Phe73, Trp77, His80, and Trp238. This result confirms the stability of the MD simulation and the strong interaction with the enzyme suggested by the total energy and RMSD plots. The plots of Fig. 14 illustrate that Val12 and His80 approach compound **6** closely enough to form hydrogen bonds, corroborating our previous findings from the docking study. As already mentioned before, interactions with these two residues compensate for the absence of Arg252 and Asp255 from the active site of *Ba*NH. Moreover, the presence and proximity of the residues Phe73, Trp77, and Trp238 are apparent in Fig. 13. Although these residues do not interact with it (according to the docking studies), they may contribute to the permanence of compound **6** inside the active site of *Ba*NH. Thus, upon analyzing the frames of the MD simulations, it appears that compound **6** probably undergoes hydrophobic interactions with Trp238 (Fig. 15), further contributing to the stabilization and retention of this compound within the active site of *Ba*NH and justifying the fact that this compound gives the best results according to both theoretical calculations and experimental data.

Docking results suggested that the best conformation of compound **6** inside *Ba*NH makes H-bonds with nine residues. MD results show that this compound is able to establish up to seven H-bonds and retains five H-bonds during the whole 6.0 ns of MD simulation, as can be seen in the plot of Fig. 16. This kind of analysis was performed for all 18 simulated systems and is in reasonable agreement with the results obtained in docking studies, thus showing that the proposed inhibitors remain well docked and stable in the active site for the simulated time.

Compound **6** also presented very stable dynamic behavior inside the *Tv*NH active site, as can be seen in the frames of Fig. 17. Interactions of the nucleobase with Arg252 and Tyr257, already predicted in the docking studies, are clearly observed as well as possible hydrophobic interactions with Trp261, similar to the one observed with Trp238 inside *Ba*NH. This result confirms the stability of the MD simulation and the strong interaction with the enzyme suggested by the total energy and RMSD plots. Also, the plots of Fig. 18 illustrate that Arg252 and Tyr257 approach compound **6** closely enough to create hydrogen bonds, corroborating our previous findings from the docking study.

Conclusions

The energies obtained in the docking studies indicated a good correlation between the theoretical and experimental data, corroborating the results of Goemine et al. [27, 28] that pointed to compound **6** as the best *Tv*NH inhibitor and highlighting it as the most promising *Ba*NH inhibitor.

MD simulations of the compounds in the active sites of *Ba*NH and *Tv*NH confirm the results from docking analyses, and they show that the proposed inhibitors remain stable inside the *Ba*NH active site throughout the simulation time; they also interact with the same residues as predicted in the docking studies.

The docking and MD results combined suggest that compound **6** is the most promising candidate for a lead compound in the design of potential *Ba*NH inhibitors. Derivatives of this compound may optimize their interactions with key amino acid residues of the active site, leading to new and more effective NH inhibitors. In fact, these derivatives should, preferably, have aromatic groups as substituents in order to explore the potential hydrophobic interactions with tryptophan residues belonging to the active site. Bulkier phamocophoric groups containing amine and carbonyl groups are also desirable as they can occupy the whole cavity, increasing the potential for interactions with Val12, Asp13, Asp38, Trp77 and His80. It is important to mention here that residues Val12 and His80, which were not previously reported to be part of the active site of *Ba*NH, were found to be very important to the stabilization of ligands inside *Ba*NH, considering that interactions with them were observed to compensate for the absence of residues equivalent to Arg252 and Asp255 in the active site of *Ba*NH.

Acknowledgments The authors wish to thank the Brazilian financial agencies Conselho Nacional de Desenvolvimento Científico e Tecnológico (CNPq), Fundação de Amparo ao Ensino e Pesquisa do Estado do Rio de Janeiro (FAPERJ), Fundação de Amparo à Pesquisa do Estado de Minas Gerais (PAPEMIG) and Coordenação de Aperfeiçoamento de Pessoal de Nível Superior/Ministério da Defesa (CAPES/MD) (Edital PRODEFESA 2008) for financial support, and the Military Institute of Engineering for providing the physical infrastructure and working space.

References

1. Goldman DL, Arturo C (2008) Anthrax-associated shock. Front Biosc 13:4009–4014
2. Sterne M (1967) Distribution and economic importance of anthrax. Fed Pro 26:1493–1495
3. Dixon TC, Meselson M, Guillemin J, Hanna PC (1999) Anthrax. N Eng J Med 341:815–826

4. Turnbull PC (1996) B. Anthrax is alive and well PHLS. Microbiol Digest 9:103–106
5. Lindler LE, Lebeda FJ, Korch GW (2005) Biological weapons defense: infectious diseases and counter bioterrorism. Humana, Totowa
6. Parkin DW, Schramm VL (1995) Binding modes for substrate and a proposed transition—state analogue of protozoan nucleoside hydrolase. Biochemistry 34:13961–13966
7. Gopaul DN, Meyer SL, Sacchettini JC, Schramm VL (1996) Inosine-uridine nucleoside hydrolase from crithidia fasciculate: genetic characterization, crystallization, and identification of histidine 241 as a catalytic site residue. Biochemistry 35:5963–5970
8. Degano M, Almo SC, Sacchettini JC, Schramm VL (1998) Trypanossomal nucleoside hydrolase. A novel mechanism from the structure with a transition-state inhibitor. Biochemistry 37:6277–6285
9. Shi W, Schramm VL, Almo SC (1999) Nucleoside hydrolase from *Leishmania major*: cloning, expression, catalytic properties, transition state inhibitors, and the 2.5-Å crystal structure. Biol Chem 274:21114–21120
10. Cui L, Rajasekariah GR, Martin SK (2001) A nonspecific nucleoside hydrolase from *Leishmania donovani*: implications for purine salvage by the parasite. Gene 280:153–162
11. Santana DM, Borja-cabrera GP, de Souza EP, Sturm NR, Palatnik CB, Campbell DA (2002) Nucleoside hydrolase from *Leishmania donovani* is an antigen diagnostic for visceral leishmaniasis. Mol Biochem Parasitol 120:315–319
12. Versées W, Steyaert J (2003) Catalysis by nucleoside hydrolases. Curr Opin Struct Biol 13:731–738
13. Ogawa J, Takeda S, Xie SX, Hatanaka H, Ashikari T, Amachi T, Shimizu S (2001) Purification, characterisation, and gene cloning of purine nucleosidase from *Ochrobactrum anthropi*. Appl Environ Microbio 67:1783–1787
14. Petersen C, Moller LB (2001) The RihA, RihB, and RihC ribonucleoside hydrolases of *Escherichia coli*. Substrate specificity, gene expression, and regulation. J Biol Chem 276:884–894
15. Kurtz JE, Exinger F, Erbs P, Jund R (2002) The URH1 uridine ribohydrolase of *Saccharomyces cerevisae*. Curr Genet 41:132–141
16. Pellé R, Schramm VL, Parkin DW (2001) Molecular cloning and expression of a purine-specific N-ribohydrolase from *Trypanosoma brucei brucei*: sequence, expression, and molecular analysis. J Biol Chem 273:2118–2126
17. Ribeiro JM, Valenzuela JG (2003) The salivary purine nucleosidase of the mosquito, *Aedes aegypti* Insect. Biochem Mol Biol 33:13–22
18. França TCC, Rocha MRM, Reboredo BM, Rennó MN, Tinoco LW, Villar JDF (2008) Design of inhibitors for nucleoside hydrolase from *Leishmania donovani* using molecular dynamics studies. J Braz Chem Soc 19:64–73
19. França TCC, Pascutti PG, Ramalho TC, Villar JDF (2005) A three-dimensional structure of *Plasmodium falciparum* serine hydroxymethyltransferase in complex with glycine and 5-formyl-tetrahydrofolate. Homology modeling and molecular dynamics. Biophys Chem 115:1–10
20. França TCC, Wilter A, Pascutti PG, Ramalho TC, Villar JDF (2006) Molecular dynamics of the interaction of *Plasmodium falciparum* and human serine hydroxymethyltransferase with 5-formyl-6-hydrofolic acid analogues: design of new potential antimalarials. J Braz Chem Soc 17:1383–1392
21. Gonçalves AS, França TCC, Wilter A, Villar JDF (2006) Molecular dynamics of the interaction of pralidoxime and deazapralidoxime with acetylcholinesterase inhibited by the neurotoxic agent tabun. J Braz Chem Soc 17:968–975
22. Silva ML, Gonçalves AS, Batista PR, Villar JDF, Pascutti PG, França TCC (2010) Design, docking studies and molecular dynamics of new potential selective inhibitors of *Plasmodium falciparum* serine hydroxymethyltransferase. Mol Simul 36:5–14
23. Ramalho TC, França TCC, Rennó MN, Guimarães AP, Cunha EFF, Kuča K (2010) Development of new acetylcholinesterase reactivators: molecular modeling versus in vitro data. Chem Biol Interact 187:436–440
24. Gonçalves AS, França TCC, Villar JDF, Pascutti PG (2010) Conformational analysis of toxogonine, TMB-4 and HI-6 using PM6 and RM1 methods. J Braz Chem Soc 21:179–184
25. Gonçalves AS, França TCC, Villar JDF, Pascutti PG (2011) Molecular dynamics simulations and QM/MM studies of the reactivation by 2-PAM of tabun inhibited human acethylcholinesterase. J Braz Chem Soc 22:155–165
26. Guimarães AP, Oliveira AA, Cunha EFF, Ramalho TC, França TCC (2011) Design of new chemotherapeutics against the deadly anthrax disease. Docking and molecular dynamics studies of inhibitors containing pyrrolidine and riboamidrazone rings on nucleoside hydrolase from *Bacillus anthracis*. J Biol Struct Dyn 28:455–469
27. Goeminne A, McNaughton M, Bal G, Surpateanu G, van der Veken P, de Prol S, Versées W, Steyaert J, Haemers A, Augustyns K (2008) Synthesis and biochemical evaluation of guanidino-alkyl-ribitol derivatives as nucleoside hydrolase inhibitors. Eur J Med Chem 43:315–326
28. Goeminne A, McNaughton M, Bal G, Surpateanu G, van der Veken P, de Prol S, Versées W, Steyaert J, Haemers A, Augustyns K (2008) N-Arylmethyl substituted iminoribitol derivatives as inhibitors of a purine specific nucleoside hydrolase. Bioorg Med Chem 16:6752–6763
29. Versées W, Decanniere K, Pellé R, van Holsbeve E, Steyaert J (2002) Enzyme-substrate interactions in the purine-specific nucleoside hydrolase from *Trypanosoma vivax*. J Biol Chem 277:15938–15946
30. Versées W, Barlow J, Steyaert J (2006) Transition-state complex of the purine-specific nucleoside hydrolase of *T.vivax*: enzyme conformational changes and implications for catalysis. J Mol Biol 359:331–346
31. Berman HM, Westbrook J, Feng Z, Gilliland G, Bhat TN, Weissig H, Shindyalov IN, Bourne PE (2000) The protein data bank. Nucleic Acids Res 28:235–242
32. Guex N, Peitsch MC (1997) SWISS-MODEL and Swiss-PdbViewer: an environment for comparative protein modeling. Electrophoresis 18:2714–2723
33. Thomsen R, Christensen MH (2006) MolDock: a new technique for high-accuracy molecular docking. J Med Chem 49:3315–3321
34. Hehre WJ, Deppmeier BJ, Klunzinger PE (1999) PC SPARTAN Pro. Wavefunction, Inc., Irvine
35. Van der Spoel D, van Buuren AR, Apol E, Meulenhoff PJ, Tieleman DP, Sijbers ALT M, Hess B, Feentra KA, Lindahl E, van Drunen R, Berendsen HJC (2001) GROMACS user manual, version 3.0. University of Groningen, Groningen
36. Schuettelkopf AW, van Aalten DMF (2004) PRODRG: a tool for high-throughput crystallography of protein±ligand complexes. Acta Crystallogr D60:1355–1363
37. Frisch MJ, Trucks GW, Schlegel HB, Scuseria ES, Pople JA et al (2001) Gaussian 98, revision A.11. Gaussian, Inc., Pittsburgh
38. Humphrey W, Dalke A, Schulten K (1996) VMD: visual molecular dynamics. J Mol Graph 14:33–38
39. Edwards PM (2002) Origin 7.0: scientific graphing and data analysis software. J Chem Inf Comput Sci 42:1270–1271

40. Koradi R, Billeter M, Wüthrich K (1996) MOLMOL: a program for display and analysis of macromolecular structures. J Mol Graph 14:51–55
41. Warren D (2002) The PyMOL molecular graphics system. DeLano Scientific, San Carlos
42. Warren GL, Webster AC, Capelli AM, Clarke B, LaLonde J, Lambert MH, Lindvall M, Nevins N, Semus SF, Senger S, Tedesco G, Wall ID, Woolven JM, Peishoff CE, Head MS (2006) A critical assessment of docking programs and scoring functions. J Med Chem 49:5912–5931
43. Leach AR, Shoichet BK, Peishoff CE (2006) Prediction of protein–ligand interactions. Docking and scoring: successes and gaps. J Med Chem 49:5851–5855
44. Kontoyanni M, McClellan LM, Sokol GS (2004) Evaluation of docking performance: comparative data on docking algorithms. J Med Chem 47:558–565